

Article

# Detection of Land Subsidence in Kathmandu Valley, Nepal, Using DInSAR Technique

Richa Bhattarai <sup>1,\*</sup>, Haireti Alifu <sup>2</sup>, Aikebaier Maitiniyazi <sup>1</sup> and Akihiko Kondoh <sup>2</sup>

<sup>1</sup> Geosystem and Biological Sciences Division, Graduate School of Science, Chiba University, 1-33 Yayoi-cho, Inage-ku, Chiba-shi, Chiba 263-8522, Japan; akbar120311@gmail.com

<sup>2</sup> Center for Environmental Remote Sensing, Chiba University, 1-33 Yayoi-cho, Inage-ku, Chiba-shi, Chiba 263-8522, Japan; hairetialifu@outlook.com (H.A.); kondoh@faculty.chiba-u.jp (A.K.)

\* Correspondence: richa\_b5@hotmail.com

Academic Editor: Paul Aplin

Received: 17 April 2017; Accepted: 6 June 2017; Published: 11 June 2017

**Abstract:** Differential Synthetic Aperture Radar Interferometry (DInSAR) is a remote sensing technique that is capable of detecting land surface deformation with centimeter accuracy. In this research, this technique was applied to two pairs of Advanced Land Observing Satellite (ALOS) Phased Array L-band SAR (PALSAR) data to detect land subsidence in the Kathmandu valley from 2007 to 2010. The result revealed several subsidence areas towards the center of the valley ranging from a maximum of 9.9 km<sup>2</sup> to a minimum of 1 km<sup>2</sup> coverage with a maximum velocity of 4.8 cm/year, and a minimum velocity of 1.1 cm/year, respectively. The majority of the subsidence was observed in old settlement areas with mixed use development. The subsidence depth was found to gradually increase from the periphery towards the center in almost all detected subsidence areas. The subsidence depth was found to be in a range of 1 cm to 17 cm. It was found that the concentration of deep water extraction wells was higher in areas with higher subsidence rates. It was also found that the detected subsidence area was situated over geological formations mainly consisting of unconsolidated fine-grained sediments (silica, sand, silt, clay and silty sandy gravel), which is the major factor affecting the occurrence of land subsidence due to groundwater extraction.

**Keywords:** land subsidence; ALOS PALSAR; DInSAR; Kathmandu valley; urban

---

## 1. Introduction

### 1.1. Background

Land subsidence is defined as an environmental geological phenomenon that causes the slow lowering of ground surface elevation [1]. It is often a result of the natural compaction of sediments and extraction of ground water, geothermal fluids, oil, gas, coal and other solids through mining [2]. Land subsidence tends to change the topographic gradients, and thus causes infrastructure damage, ruptures in the land surface, aggravates flooding, causes inundation of land and reduces the capacity of aquifers to store water; ultimately posing a risk for society and the economy [3]. The occurrence of land subsidence has been studied in many places around the world, including Tokyo, Japan [4]; Mexico [5]; Saudi Arabia [6]; Texas, USA [7]; Jakarta, Indonesia [8]; Ravenna, Italy [9]; Bangkok, Thailand [10,11]; Pingtung Plain, Taiwan [12]; and China [13].

The driving force behind land subsidence is mainly a combination of a primary factor and an immediate factor; the primary factor being the existence of unconsolidated sediment deposits that comprise the aquifer system, and the immediate factor being the diminishing groundwater level [14–16]. An area is potentially prone to land subsidence if a thick sediment deposit prone to consolidation exists in the subsoil, along with water which is susceptible to being pumped. Lowering of the water

table due to groundwater harvesting is the triggering factor of subsidence [17]. Nonetheless, even if the water table is reduced, land subsidence will not occur if the aquifer system lacks the presence of unconsolidated sediments. It has been found that excessive groundwater exploitation can result in a slow, but eventually significant, land subsidence [1,18–21]. A close relationship between the amount of groundwater withdrawal for industrial activities and advancement of land subsidence was recognized early in Japan during observations made between 1954 and 1960 [22]. Additionally, geology also plays a vital role in the acceleration of land subsidence. Large amounts of groundwater extraction from certain types of underlying sediments, such as fine-grained sediments, result in compaction of these sediments, because the groundwater is partly responsible for the subsurface support. This ultimately triggers land subsidence [23].

Kathmandu is a bowl-shaped valley with two principle landforms—alluvial and flood plains—making it even more prone to subsidence. Groundwater has always been a significant source of the water supply in the Kathmandu valley since the early 1970s [24]. As the water demand started exceeding the supply, private and governmental institutions started to pump groundwater through private wells. Visible impacts on water levels were observed during the mid-eighties, when the Nepal Water Supply Corporation (NWSC) started including groundwater into its supply system [25]. During the nineties, the number of private wells increased so rapidly that the extraction exceeded the water recharge levels. The constantly increasing population, industrialization and urbanization have triggered the increase in groundwater consumption. Extraction of groundwater has increased from 2.3 million-liters-a-day (MLD) in 1979 to 80 MLD in 2011 [26]. Groundwater fulfills nearly 50% of the total water demand during the wet season and 60–70% during the dry season [27]. Consequently, annual extraction exceeds recharge, leading to tremendous depletion in groundwater levels. With an ever-increasing population, development activities and a lack of groundwater resource policy, the water demand is bound to exerting increasing pressure on the groundwater table. This, in turn, will result in aquifer compaction in areas consisting of highly compressible clay and silt layers, raising the risk of land subsidence [28]. Also, considering the relation of groundwater exploitation and land subsidence from the case studies of various countries, it can be assumed that the same may occur in the Kathmandu valley, as well. Nonetheless, no published research has been done, to the authors' knowledge, to determine if land subsidence is actually taking place to ground water extraction; therefore, no evidence of land subsidence in the Kathmandu valley is available [24].

Research has been done focusing on the land deformation caused by the crustal movements in the region. On 25 April 2015, a devastating earthquake of Mw 7.8 struck central Nepal. It was followed by a strong aftershock of Mw 7.3 on 12 May 2015, and many other aftershocks greater than Mw 6 thereafter. This earthquake was a result of stress released from the under thrust movement of the Indian tectonic plate beneath the Eurasian tectonic plate [29]. The earthquake ruptured the Main Himalayan Thrust fault (MHT), which stopped halfway at 11 km under the Kathmandu valley. Therefore, there are chances of a future fault rupture on the surface [30]. Uplift of approximately 1 m was observed 20 km northeast of Kathmandu city at longitude/latitude 27.74/85.50°, and local subsidence was observed to the north of the city [29,31]. The data inventory of the historical occurrence of great Himalayan earthquakes is sporadic, due to the complexity of evaluating these events [31–33]. Also, the rupture location identity and the return time is difficult to predict [34]. Therefore, it is difficult to conduct seismic hazard assessment in highly-populated regions near the Himalayas [35].

It was only after this event that a few works mentioned subsidence, with the sole cause being the earthquake [29,36]. A developing country, recently struck by a natural disaster, is rebuilding; and if subjects like land subsidence, which have been troubling the globe, are not addressed immediately, then the consequences could be unaffordable. Therefore, mapping, continuous monitoring and risk assessment of land subsidence is critical in a place like the Kathmandu valley.

Differential Synthetic Aperture Radar interferometry (DInSAR) is an advanced remote sensing tool that has the ability to map displacements over vast areas at a very high spatial resolution, at a lower cost than other conventional techniques, such as GPS, topographic measure and

extensometers [37]. Previously, several researchers have applied this method to map and monitor groundwater extraction-induced subsidence all around the world with successful results. For example, in Antelope Valley, California [38]; Coachella Valley, California [39]; Kolkata, India [40]; Iran [41]; Jakarta [42]; and Alto Guadalentin Basin, Spain [43].

### 1.2. Relevant Literature

Land subsidence has been a global problem for a very long time. Many studies have and are being conducted throughout the world by applying remote sensing techniques [2,37–40,42,44–48]. Reviewing case histories of geologically similar areas can give the impression of a possible land subsidence trend. Some similar studies are as follows:

A study conducted by Strozzi et al., 1999 [2] in a valley of Mexico City that is built on highly compressible lacustrine clays with high ground water extraction values showed results of land subsidence velocity of more than 30 cm/year in some areas. Seven ERS-1/2 SAR images pairs from December 1995 to September 1997 were processed using differential SAR interferometry to map land subsidence.

Amelung et al., 1999 detected land subsidence in Las Vegas, Nevada, United States between 1992 and 1997 by using InSAR technique. A maximum subsidence of 19 cm during the observation period was observed by utilizing two SAR images acquired by the ERS satellite. The study also concluded that the extent of the subsidence was dependent on the geological structure and sediment composition of the location [49].

Another study conducted by Boni et al. [43] in 2015 revealed that the Alto Guadalentin Basin in southern Spain had up to 2.5 m cumulated subsidence between 1992 and 2012. The DInSAR technique was applied to four datasets of SAR images obtained from ERS-1/2, ENVISAT, ALOS and COSMO-SkyMed satellites to obtain land subsidence evolution within a twenty-year period. It was found that the ground displacement was directly correlated with the thickness of the compressible alluvial deposits. The authors also suggest that the detected land subsidence over the past 20 years is a consequence of 100–200 m groundwater drop caused by overexploitation of the Alto Guadalentin aquifer system.

A study conducted by Calo et al., 2015 in Istanbul Megacity, Turkey, where the major geological constituents are mainly composed of clay, sand, gravel and silt, revealed subsidence occurrence over urbanized areas during the observation period of 2010–2012. The SBAS (Small Baseline Subset) DInSAR technique was applied to 43 TerraSAR-X data, which revealed an average subsidence velocity of 3 cm/year, with most of the detected subsidence found to be occurring in the Quaternary layers [50].

### 1.3. Scope

Little is known about land subsidence, and very few studies are being conducted, in Nepal. Therefore, the outcome of this research will help build our understanding of the current situation, allowing the development of prevention techniques and risk management. After verifying the accuracy of this result by comparing it with land measurement data and field survey, it is expected that it will be useful for the government and interested stakeholders for the promotion of a better understanding of the situation for sustainable development and policy-making for disaster prevention.

The results from this study could serve as a significant benchmark for the Kathmandu Valley, Nepal, as it is developing towards sustainable urbanization, but lacks proper data and research.

### 1.4. Objective

The main objective of this research is to detect land subsidence in the Kathmandu valley by the application of the Differential Synthetic Aperture Radar Interferometry (DInSAR) technique to Advanced Land Observing Satellite (ALOS) Phased Array L-band Synthetic Aperture Radar (PALSAR) data.

## 2. Materials and Methodology

### 2.1. Study Area

The Kathmandu valley, the largest urban agglomerate of Nepal, is located between  $27^{\circ}34'33''$  and  $27^{\circ}49'4''$  N latitudes and  $85^{\circ}11'19''$  and  $85^{\circ}34'57''$  E longitudes, covering an area of  $654.7 \text{ km}^2$ . The valley consists of three major cities: namely, Kathmandu, the capital city; Bhaktapur and Lalitpur, ancient cultural gem cities. The population density is 2793 people per square kilometer as of the 2011 census. The average elevation is approximately 1400 m above sea level. This bowl-shaped valley is filled with more than 550 m thick lacustrine and fluvial deposits [51], which make it prone to land subsidence. The Landsat image of the Kathmandu valley is shown in Figure 1.

Geology of the Kathmandu valley: the Kathmandu valley is surrounded by the Shivapuri mountain range (2732 m) in the North, the Phulchauki mountain range (2762 m) in the south, the Nagarkot mountain range (1895 m) in the east and the Chandragiri mountain range (2356 m) in the west [52]. The main geological composition of the Kathmandu valley is quaternary sediment over basement rock [53]. The basement rock is formed by Precambrian to Devonian rocks, which mainly consist of limestone, dolomite, slate, metasandstone, phyllite, marble, schist, quartzite and garnet-schist [54]. The quaternary sediment consists of thick (more than 650 m deep), semi-consolidated fluvio-lacustrine sediments from the Pliocene to the Pleistocene age [54]. It is composed of fine-to coarse-grained sand, gravel, clay, silt, peat, lignite and diatomite [55]. The geological map of the Kathmandu valley is shown in Figure 2.

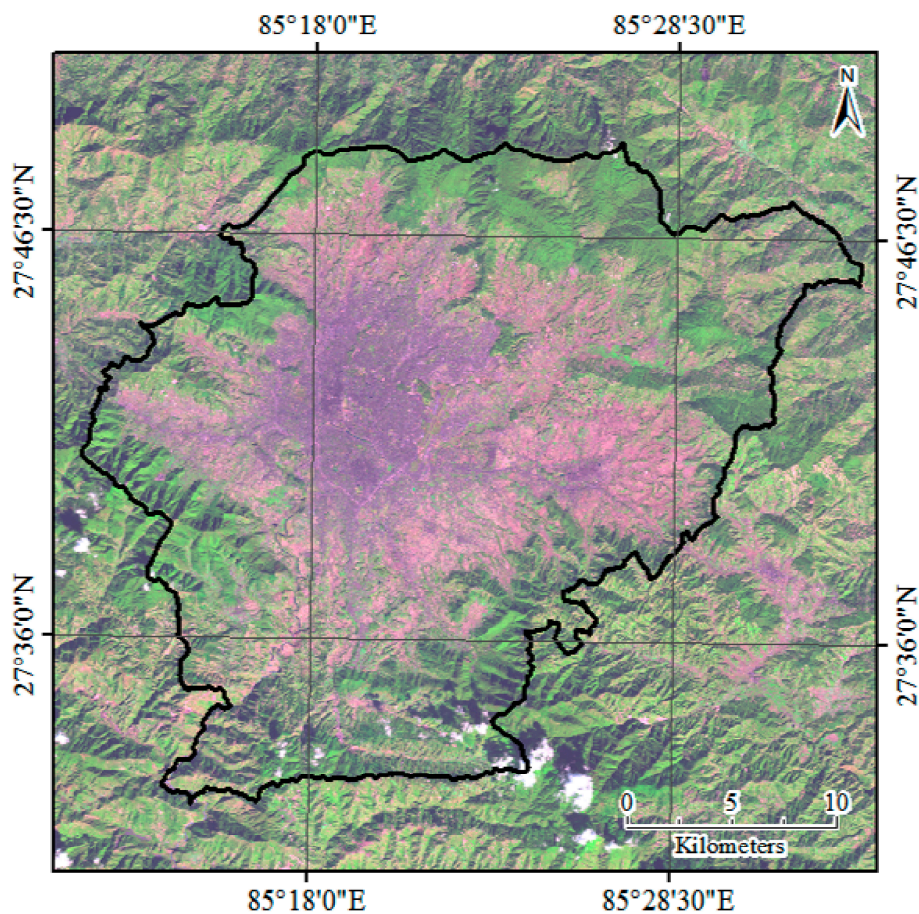


Figure 1. Landsat Image of the Kathmandu valley, observed on 10 November 2016.

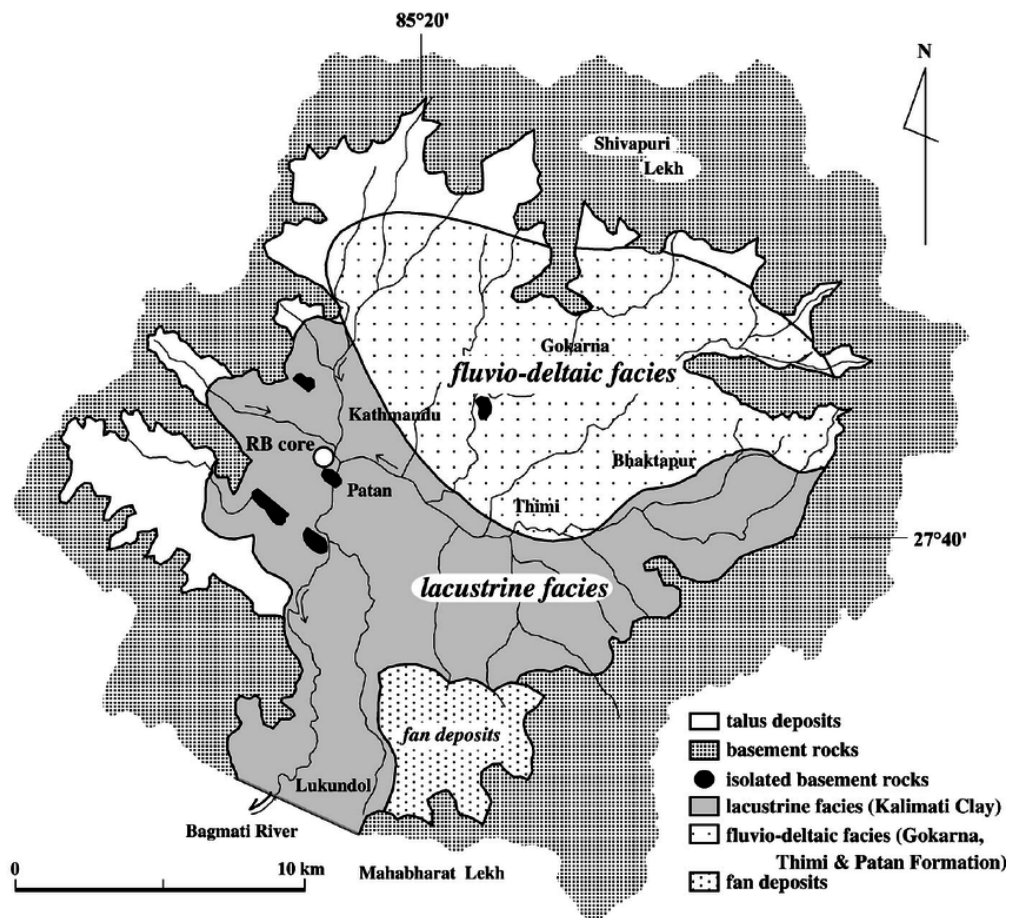


Figure 2. Geological map of the Kathmandu basin (Source: [56]).

2.2. Data

Three ALOS PALSAR fine-mode, single-polarization data, acquired at different acquisition times between 2007 and 2010 with identical observation parameters—like path/row 510/54, off nadir angle  $34.3^\circ$ —were selected for this research. The details of the two pairs generated from this data are shown in Table 1, below. Since a perpendicular baseline value between 150 to 450 m gives the best interferogram result [57], this factor was also considered while selecting the pairs of images. The data used in this research was purchased from Japan Space Systems.

Also, a Digital Elevation Model (DEM) was extracted from Shuttle Radar Topography Mission (SRTM) 1 Arc second (resolution of 30 m) global elevation data. This data was downloaded from theEarth explorer data portal.

Table 1. ALOS PALSAR data pair information.

InSAR Pair	Observation Date	Interval (Days)	Perpendicular Baseline (m)
Pair 1	2 November 2007	138	417
	19 March 2008		
Pair 2	2 November 2007	828	257
	7 February 2010		

### 2.3. Methodology

Synthetic Aperture Radar (SAR) is a system able to obtain high-resolution, complex images from wide areas of terrain, usually located on board an orbital or airborne platform, but also useable in ground based deployments [58]. DInSAR is a remote sensing technique useful for detecting land displacement or deformation accurately for a wide coverage area by utilizing the phase difference between two or more sets of SAR data taken at different acquisition times. The phase difference between an interferometry data pair can be expressed as follows:

$$\text{Int} = \varphi_{\text{disp}} + \varphi_{\text{atm}} + \varphi_{\text{noise}} + \varphi_{\text{topo}} + \varphi_{\text{flat}} \quad (1)$$

where  $\varphi_{\text{disp}}$  refers to the phase difference from ground displacement along the slant range;  $\varphi_{\text{atm}}$  refers to the atmospheric effect;  $\varphi_{\text{noise}}$  refers to the noise from the radar instrument and temporal deceleration;  $\varphi_{\text{topo}}$  refers to the topographic height information; and  $\varphi_{\text{flat}}$  refers to the assumption of an ideally flat earth terrain [42]. In the DInSAR technique, the ground displacement is estimated to be in a slant range direction; therefore, Equation (2) can be used to obtain ground displacement in a vertical direction [59].

$$\Delta z = \Delta s l \cos \theta \quad (2)$$

where  $\Delta z$  is ground displacement in a vertical direction;  $\Delta s l$  is ground displacement in a slant range; and  $\theta$  is the incidence angle, which is assumed to be  $34.3^\circ$ , which is as same as the sensor's off-nadir angle.

In this study, the DInSAR technique was performed using the SARSCAPE module in ENVI software to detect land subsidence in the Kathmandu valley. The method of DInSAR processing is explained step by step as follows:

*Focusing:* The purpose of this first step is to collect the energy dispersed in both azimuth and range directions in the raw (level 1.0 product) ALOS PALSAR data into a single pixel (i.e., Single Look Complex (SLC) image), which can be used for further processing.

*Multilooking and Co-registration:* In this step, the SLC images are divided into different looks, characterized by different frequencies in order to reduce the speckle due to constructive and destructive interferences between the different backscattered signals from the different ground targets [60]. Image co-registration is the process of superimposing two or more SAR images in the slant range geometry. [61].

*Interferogram Generation and Flattening:* After image co-registration, where the master and slave images are precisely overlaid with an accuracy within fractions of a pixel to compute the phase difference between them, an interferometric phase is generated by multiplying the master image by the complex conjugate of the slave image. The variable viewing angles of the terrain can cause range spectra shifts, and the different Doppler can cause azimuth spectra shifts. An azimuth filter is applied during the interferogram generation to fully capture the scene's potential coherence [61]. The constant height of the terrain results in parallel (flat earth) fringes along the range direction in the generated interferogram. A pre-existing DEM of 30 m resolution from SRTM is applied to simulate the topographic phase to obtain a flattened interferogram.

*Adaptive Filtering and Coherence Generation:* The noise from radar instruments and temporal deceleration is removed by applying the Goldstein-Werner filtering process to the noisy interferogram [62]. Coherence is a measure of interferogram quality. It is calculated as the ratio between coherent and incoherent summations of two co-registered SAR images. A coherence value approaching 1 suggests that the two pixels are correlated and there is no phase noise; whereas a coherence value of 0 (black = 0) suggests that the two pixels are decorrelated and there is phase noise, and thus should not be considered for further processing.

*Phase Unwrapping:* The flattened and filtered interferogram obtained from the earlier processing always has a phase value within a range of 0 to  $2\pi$ , which means that every time the phase change

exceeds  $2\pi$ , the phase value starts with 0 again and the cycle repeats itself. This is called  $2\pi$  ambiguity and phase unwrapping resolves this problem.

*Refinement and Reflattening:* Orbital correction has great significance for the accurate transformation of phase information to height information. Therefore, Ground Control Points appointed on DEM are used to calculate the absolute phase, and refine the orbits.

*Phase to Displacement Conversion and Geocoding:* The obtained phase information is converted into displacement using Equations (1) and (2), and is finally projected onto a standard geographic coordinate system, thus generating a displacement map.

### 3. Result and Discussion

The coherence image of each pair for the study area is shown in Figure 3. A coherence value close to 1 (i.e., white color) indicates that there is no phase noise, whereas a coherence value of 0 (i.e., black color) indicates that there is only phase noise. Areas with high coherence (coherence value 1) display clear interferogram patterns in the interferogram image, whereas areas with low coherence (coherence value 0) displays noisy interferogram patterns. Good coherence is seen in both of our pairs; therefore, they can be considered for interferogram generation.

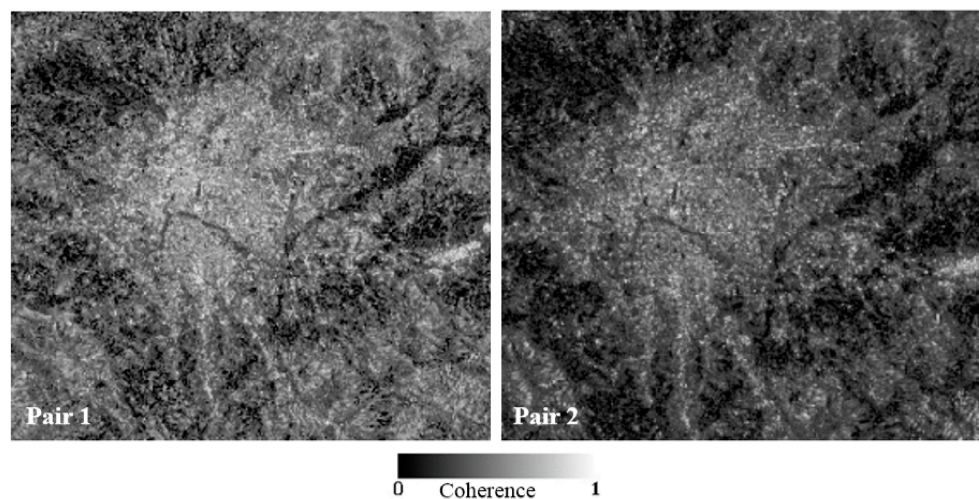


**Figure 3.** Coherence image of Pair 1 (2 November 2007 and 19 March 2008) and Pair 2 (2 November 2007 and 7 February 2010) obtained from DInSAR processing.

The DInSAR interferogram of the Kathmandu valley for the observation interval 2 November 2007 to 7 February 2010 is shown in Figure 4. Interferogram fringes can be seen in various areas which indicates the occurrence of land deformation. An area where the color turns from blue to pink to yellow to green is considered to be affected by land subsidence, whereas the area where the color turns from blue to green to yellow to pink is considered to be affected by land uplift. Figure 4 clearly indicates the occurrence of land subsidence. It is noticeable that some fringes on the south-eastern part do not display clear patterns. This is because interference cannot easily occur in inclined ground surfaces, and this part of the study area is a hilly region.

Figure 5 shows the subsidence contour with displacement values in centimeters for the land subsidence-affected areas, which are indicated by points L1–L8. A significant linear feature striking NW–SE can be seen in Figure 5. The pattern displayed by ground deformations may depict the underlying structural arrangement of a location [63]. Referring to Figures 2 and 9, it can be said that the subsidence pattern obtained here is modulated by the underlying sediments. Clear linear features can be observed parallel to the fluvio-deltaic facies and lacustrine facies boundary.

Location L1, in central Kathmandu, shows the maximum amount of subsidence (17 cm). It is a mixed-use development area (a type of urban development that comprises an amalgamation of

residential, commercial, cultural, institutional, and/or industrial uses, along with their physical and functional integration, including pedestrian connections [64]). Location L2—Chauni and periphery—is an old settlement area with an army camp and ancient museum covering most of the subsidence zone. Location L3—Lalitpur—is also an old mixed-use settlement area. Location L4—Imadol and periphery—is a location on the outskirts of the Kathmandu city urban center, which is gradually changing from farmland/cropland into urban land use. This location also has a small number of brick kilns, which might be affecting the ground surface elevation. Location L5—Thimi and periphery—is a mixed-use settlement area with croplands on the north-eastern side of the subsidence zone. Location L6—Madhyapur Thimi—is mostly cropland with a few residential areas (spots), but is gradually being urbanized by land plotting. Location L7—New Baneshwor and Koteshwor—are also mixed-use settlement areas, with the majority being commercial buildings. Location L8—Gothatar—mostly consists of croplands with a few residential buildings, along with a small northern portion of the international airport runway. The outskirts of the valley are mostly rural, but urbanization is slowly spreading from the center of the valley towards the periphery. A Google Earth image displaying portions of location is shown in Figure 6.

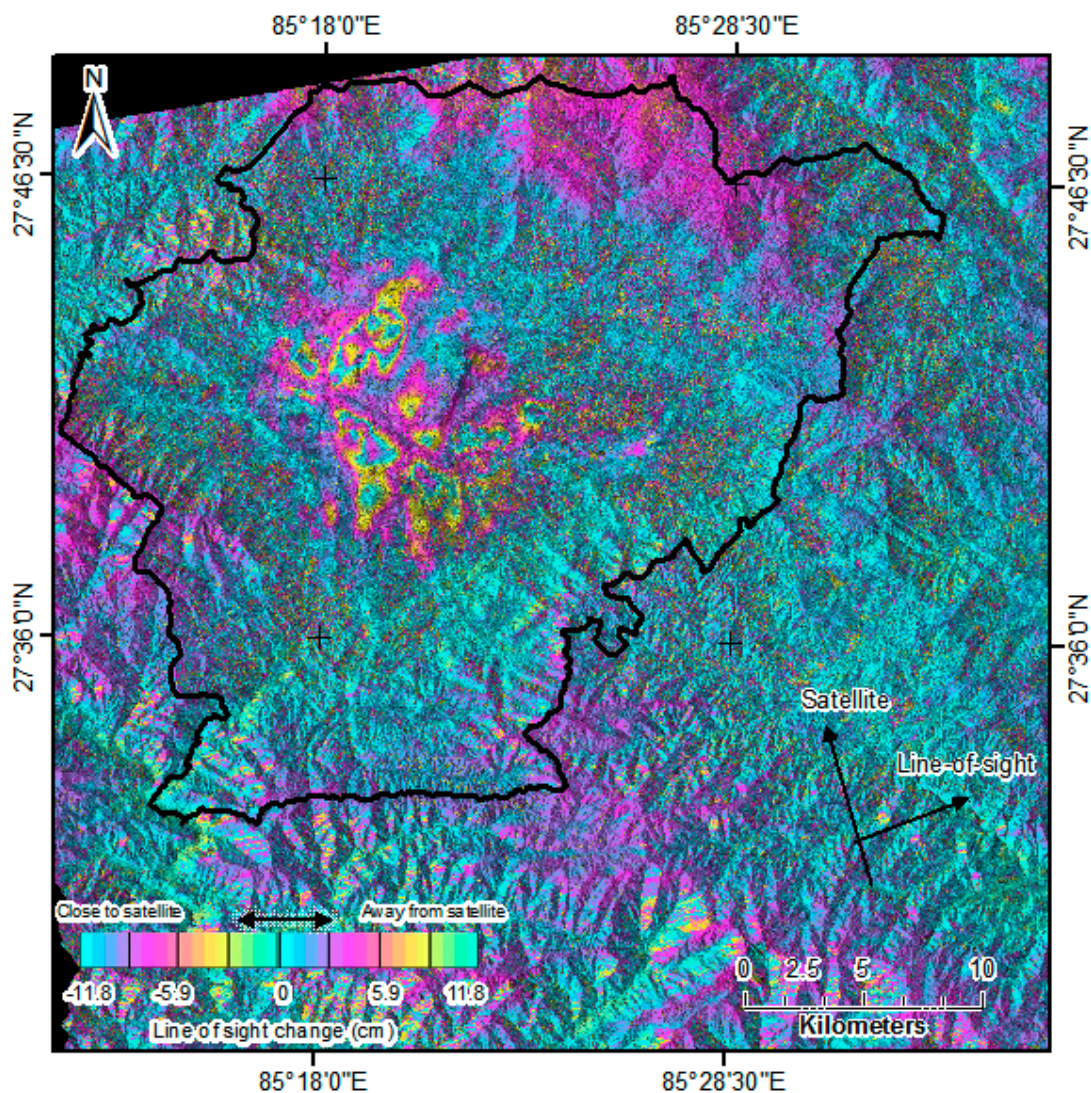


**Figure 4.** Differential interferogram for Kathmandu Valley from 2 November 2007 to 7 February 2010 obtained from DInSAR processing.

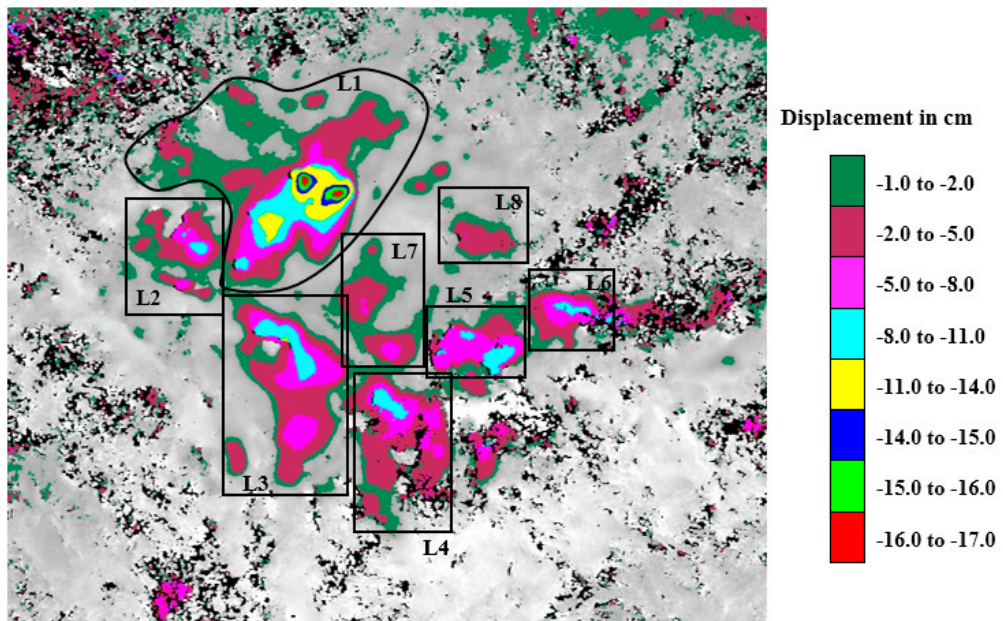


Figure 5. Subsidence contour showing displacement values in centimeters.

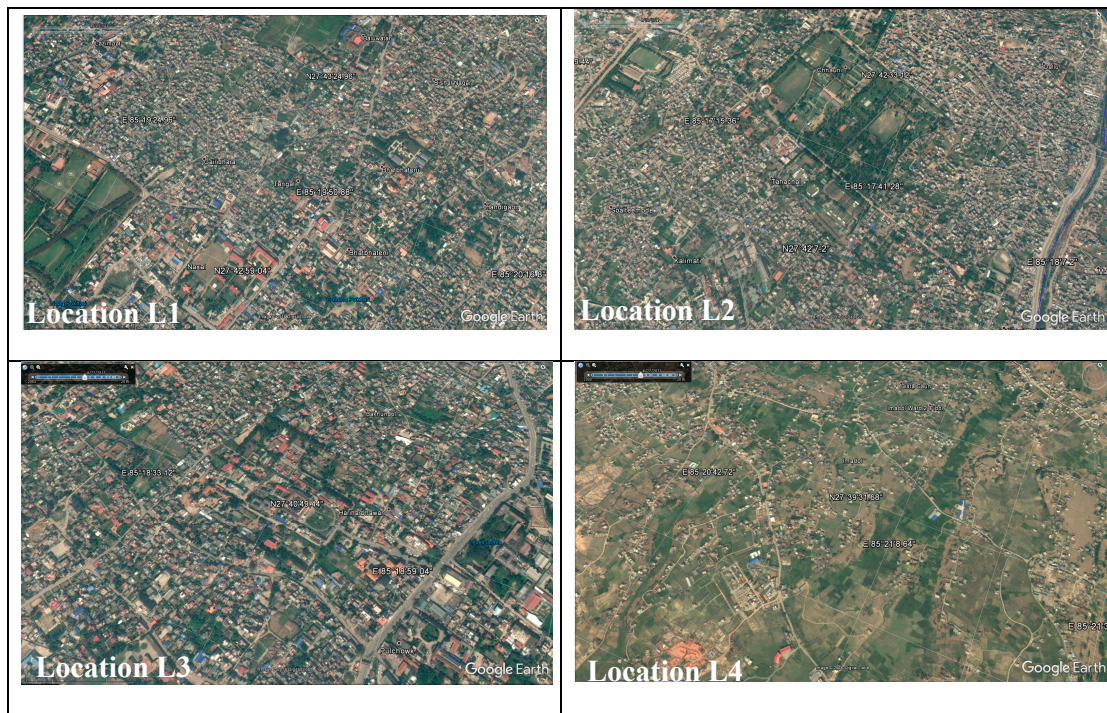


Figure 6. Cont.



Figure 6. Google Earth images from the year 2011 showing portions of land subsidence Locations L1 to L8.

Figure 7 shows the location of destroyed structures as a result of the Mw 7.8 2015 Gorkha Earthquake. Maximum destruction can be observed in the location corresponding to the maximum subsidence (i.e., Location L1) whereas other locations show less destruction. The factor contributing to this might also be the fact that Location L1 consists of portions of very old settlement area where old, weak buildings were abundant.

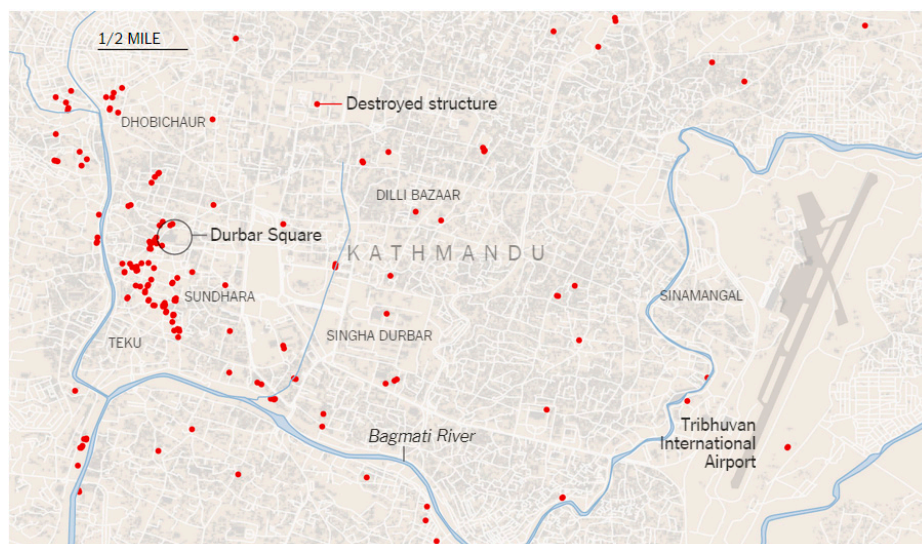


Figure 7. Grading map showing the location of destroyed structures due to 2015 Gorkha earthquake indicated by red dots. (Source: European Commission Copernicus Emergency Management Service).

The subsidence coverage area and maximum subsidence depth of each location is shown in Table 2. Subsidence depths less than 2 cm have not been considered when calculating the coverage area.

**Table 2.** Detailed information of areas affected by land subsidence.

Location Point	Location Name	Location Specification	Subsidence Coverage Area (km <sup>2</sup> )	Maximum Subsidence Depth (cm)
L1	Central Kathmandu	Mixed-use development	9.9	17
L2	Chauni	Old Army Camp	2.5	11
L3	Lalitpur	Mixed-use development	7.7	14
L4	Imadol	Residential and cropland with few brick kilns	5.7	11
L5	Thimi	Mixed-use development	3.0	11
L6	Madhyapur Thimi	Mixed-use development	2.0	11
L7	New Baneshwor and Koteshwor	Mixed-use development	2.1	8
L8	Gothatar	Residential and cropland with portion of airport runway	1.0	5

*Comparison with groundwater:* the Kathmandu valley generally consists of three hydrogeologic layers: namely, shallow aquifer, aquitard and deep aquifer. The shallow aquifer is thicker towards the north of the valley's groundwater basin, whereas the deep aquifer is thicker towards the central and southern part. The main natural recharge area is towards the northern part, and a small area contributing to recharge is located towards the southern part [24]. Locations L1, L7 and L8 lie on the northern part of the groundwater basin, where the shallow aquifer is thicker; whereas Locations L3, L4, L5 and L6 lie on the central and southern part of the groundwater basin, where the deep aquifer is thicker. As mentioned in the background, earlier, the Kathmandu valley mainly relies on groundwater as the main source of water. According to the Kathmandu Valley Water Supply Management Board, the use of deep tube-well pumps for water extraction from deep aquifers is dominant throughout the valley. The depth of deep tube wells mainly lies in a range of 30 to 300 m, and the daily discharge ranges from 3000 liters per day to 400,000 liters per day. Figure 8 shows the locations of registered deep tube wells in the Kathmandu valley. We can see that the concentration of wells is denser at Location L1 where the subsidence is highest, and sparse in other locations where the subsidence amount is lower. However, there are many unregistered wells throughout the valley with no information on their depth and discharge, which makes it difficult find an exact relation. Nonetheless, considering the density of urban build-up (refer to Figure 6), it can be assumed that the concentration of deep tube wells will be higher at Locations L1, L2, L3 and L7. Also, the occurrence of land subsidence is a combined effect of groundwater extraction and vulnerable hydrogeology, which might result in subsidence at places other than the site of extraction [65]. Therefore, comprehensive study of the groundwater extraction and recharge ability of the aquifer, which has not been included in this research, should be done in order to find the exact relationship.

However, it has been found through various literature reviews that extensive water extraction is one of the main causes of land subsidence. From the results obtained from this research, we can consider that water extraction does have a relation with land subsidence. But detailed study needs to be done to find the exact cause, as land subsidence is a very complex phenomenon, affected by various factors.

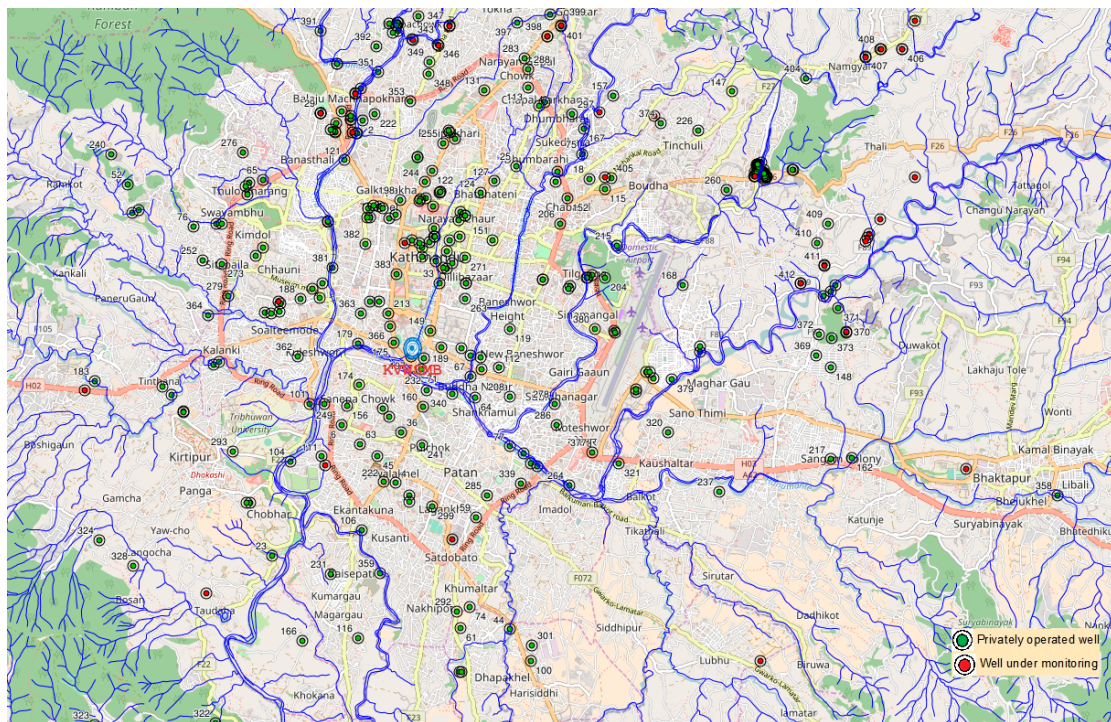


**Figure 8.** Location of registered deep well in Kathmandu Valley. (Source: Kathmandu valley water supply management board).

*Comparison with geology:* The land subsidence map generated by DInSAR processing in this research was compared briefly with the geological map of the Kathmandu valley. Figure 9 shows the subsidence contour map overlaid on the geological map of the Kathmandu valley. The maximum amount of subsidence (indicated by the red color in Figure 5) can be seen over the Gokarna Formation. This formation is mainly composed of a sands terrace from fluvio-lacustrine origins [55]. Also, a thick array of sandy and silty sediments without clay content was observed from the extensive borehole data of this formation [66]. Similarly, Locations L5, L7 and L8 are also situated over the Gokarna Formation. Locations L2, L4, L6 and small portions of Locations L3 and L7 are situated over the Kalimati Formation. Kalimati is a local name for black clay. According to Sakai (2001) [66], the predominant constituent of this formation is dark grey carbonaceous and diatomaceous (naturally occurring, soft siliceous sedimentary rock that is easily crumbled into a fine white to off-white powder) beds of open lacustrine rocks that are widely distributed underneath the surface of the central portion of the Kathmandu valley. It can also be seen in Figure 9 that a larger portion of Location L3 is situated over the Chapagaon Formation. This formation consists of somewhat rounded silty sandy gravel, occasionally with a boulder bed covered with a layer less than 1 m thick of clayey silt and silty sand [67].

From the above description, it can be summarized that land subsidence was observed mainly over three kinds of geological formations; namely, Kalimati, Gokarna and Chapagaon Formations. The main constituents of these formations are silica, sand, silt, clay and silty sandy gravel. As mentioned in relation to the mechanisms of land subsidence earlier, the major factor in occurrence of land subsidence due to ground water extraction is the presence of unconsolidated fine-grained sediments—mainly clay and silt—in an aquifer system. Hence, the relationship between geology and land subsidence occurrence can be established from this study.

These constituents are the main contents of the geology of the Kathmandu valley, and are spread throughout the valley, with the result being that the primary factor (i.e., geology) for subsidence occurrence is prevalent. Therefore, it can be said that the triggering/immediate factor (i.e., groundwater

characteristics) for subsidence occurrence is the major factor that determines the occurrence of land subsidence in the study area.

Nevertheless, land subsidence is a complex phenomenon, and this research is just a preliminary study that intends to provide basic evidence of land subsidence in the study area. This study can serve as a base for more comprehensive study in the future.

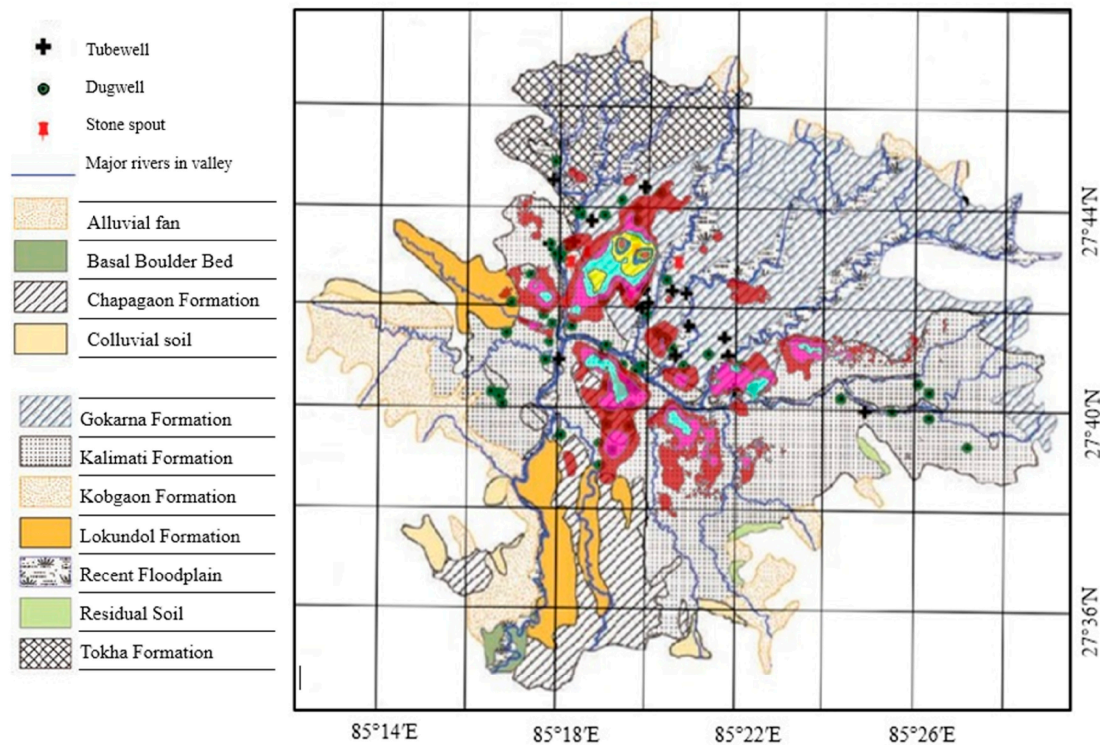


**Figure 9.** Subsidence contour overlaid on a geological map of the Kathmandu valley. (Geological map adapted from an engineering and environmental geological map of the Kathmandu valley, Department of Mines and Geology, Government of Nepal by [68].

#### 4. Conclusions

Land subsidence occurrence in the urban Kathmandu valley was detected by the application of the Differential Synthetic Aperture Radar Interferometry (DInSAR) technique to Advanced Land Observation Satellite Phased L-band SAR (ALOS-PALSAR) data. Most of the subsidence was found to have occurred in the center of the valley, where the population density is relatively higher than the surroundings. Also, the majority of the subsidence region comprised mixed-used development areas, where ground water extractions can be assumed to be at higher levels. The generated subsidence map was further studied on the basis of groundwater extraction and the geology of the Kathmandu valley. It was found that the concentration of groundwater discharge units was higher in locations detected to have high amounts of subsidence. Due to the complex nature of subsidence occurrence, and the involvement of many factors in such phenomena, detailed study is required to find the exact cause. Also, due to the non-existence of previous land subsidence measurement data and the difficulty of obtaining the GPS measurement data, the subsidence results were not able to be validated. In spite of this, the results can be considered acceptable, owing to the fact that DInSAR is a well-established methodology known to give accurate results for land deformation in urban areas.

However, very little study has been done in Nepal as of now, so the result of this research can serve as a basis for many further detailed studies. DInSAR was applied to ALOS PALSAR data to detect land subsidence in the Kathmandu valley because ALOS PALSAR covers a large area, and since no study relating to land subsidence had previously been conducted in the study area, it would serve

as the best option for identifying subsidence zones. Now that this study reveals the areas affected by subsidence, Persistent Scatterer InSAR technique can be used to obtain subsidence values in the affected areas with millimeter accuracy. Also, other SAR data with shorter wavelengths, like X-band or C-band can be used to focus on the area most affected. Also, in this study, only a few pairs of SAR data were used; using more pairs of SAR data would provide better coherence, resulting in more accurate outcomes.

**Acknowledgments:** The first author would like to express sincere gratitude to the Ministry of Education, Culture, Sports, Science and Technology (MEXT)—Super Global University (SGU), Japanese government scholarship for financially supporting the educational expenses during the period of this research. A special thanks to Ryutaro Tateishi for his valuable guidance and supervision throughout and for purchasing the required data. The authors would also like to thank the Kathmandu Valley Water Supply Management Board for providing water extraction information. Also, a hearty thanks to Ayihumaier Halipu and all the members of Tateishi lab and Kondoh lab for their constant suggestions and help throughout.

**Author Contributions:** Richa Bhattarai conceived, designed and performed the research; Hairiti Alifu and Aikebaier Maitiniyazi contributed in parts of analysis and helped with the analysis tools; Hairiti Alifu and Aikebaier Maitiniyazi also gave valuable suggestions for improving the manuscript; Akihiko Kondoh supervised the research throughout and gave valuable suggestions for improving the results and manuscript; Richa Bhattarai wrote the paper.

**Conflicts of Interest:** The authors declare no conflict of interest.

## References

- Hu, B.; Wang, J.; Chen, Z.; Wang, D.; Xu, S. Risk assessment of land subsidence at Tianjin coastal area in China. *Environ. Earth Sci.* **2009**, *59*, 269–276. [[CrossRef](#)]
- Strozzi, T.; Wegmuller, U. Land subsidence in Mexico City mapped by ERS differential SAR interferometry. In Proceedings of the International Geoscience and Remote Sensing Symposium (IGARSS), Hamburg, Germany, 28 June–2 July 1999.
- Holzer, T.L.; Galloway, D.L. Impacts of land subsidence caused by withdrawal of underground fluids in the United States. *Rev. Eng. Geol.* **2005**, *XVI*, 87–99.
- Yamaguchi, R. Water level change in the deep well of the University of Tokyo. *Bull. Earthq. Res. Inst.* **1969**, *47*, 1093–1111.
- Adrian, O.G.; Rudolph, L.D.; Cherry, A.J. Analysis of long-term land subsidence near Mexico City: Field investigations and predictive modelling. *Water Resour. Res.* **1999**, *35*, 3327–3341.
- Bankher, K.A.; Al-Harhi, A.A. Earth fissuring and land subsidence in Western Saudi Arabia. *Nat. Hazards* **1999**, *20*, 21–42. [[CrossRef](#)]
- Gabrysch, R.K.; Neighbors, R.J. Land-surface subsidence and its control in the Houston–Galveston region, TX, 1906–1995. In Proceedings of the 6th International Symposium Land Subsidence, Ravenna, Italy, 2 September 2000; pp. 81–92.
- Abidin, H.Z.; Djaja, R.; Darmawan, D.; Hadi, S.; Akbar, A.; Rajiyowiryono, H.; Sudibyoy, Y.; Meilano, I.; Kasuma, M.A.; Kahar, J.; et al. Land subsidence of Jakarta (Indonesia) and its geodetic monitoring system. *Nat. Hazards* **2001**, *23*, 365–387. [[CrossRef](#)]
- Teatini, P.; Ferronato, M.; Gambolati, G.; Bertoni, W.; Gonella, M. A century of land subsidence in Ravenna, Italy. *Environ. Geol.* **2005**, *47*, 831–846. [[CrossRef](#)]
- Bergado, D.T.; Nutalaya, P.; Balasubramaniam, A.S.; Apaipong, W.; Chang, C.C.; Khaw, L.G. Causes, effects and predictions of land subsidence in AIT campus Chao Phraya Plain, Bangkok, Thailand. *Bull. Assoc. Eng. Geol.* **1987**, *25*, 57–81. [[CrossRef](#)]
- Phien-wej, N.; Giao, P.H.; Nutalaya, P. Land subsidence in Bangkok, Thailand. *Eng. Geol.* **2006**, *82*, 187–201. [[CrossRef](#)]
- Hu, J.C.; Chu, H.T.; Hou, C.S.; Lai, T.H.; Chen, R.F.; Nien, P.F. The contribution to tectonic subsidence by groundwater abstraction in the Pingtung area, southwestern Taiwan as determined by GPS measurements. *Quat. Int.* **2006**, *147*, 62–69. [[CrossRef](#)]
- Xu, Y.S.; Shen, S.L.; Cai, Z.Y.; Zhou, G.Y. The state of land subsidence and prediction approaches due to groundwater withdrawal in China. *Nat. Hazards* **2008**, *45*, 123–135. [[CrossRef](#)]

14. Holzer, T.L. Ground failure induced by ground-water withdrawal from unconsolidated sediments. *Geol. Soc. Am. Rev. Eng. Geol.* **1984**, *VI*, 67–105.
15. Budhu, M.; Adiyaman, I.B. Mechanics of land subsidence due to groundwater pumping. *Int. J. Numer. Anal. Methods Geomech.* **2010**, *34*, 1459–1478. [[CrossRef](#)]
16. Galloway, D.L.; Burbey, T.J. Review: Regional land subsidence accompanying groundwater extraction. *Hydrogeol. J.* **2011**, *19*, 1459–1486. [[CrossRef](#)]
17. Martínez, J.P.; Cabral-Cano, E.; Wdowinski, S.; Marín, M.H.; Ortiz-Lozano, J.A.; Zerméño-de-León, M.E. Application of InSAR and gravimetry for land subsidence hazard zoning in Aguascalientes, Mexico. *Remote Sens.* **2015**, *7*, 17035–17050. [[CrossRef](#)]
18. Pratt, W.E.; Johnson, D.W. Local subsidence of the Goose Creek oil field. *J. Geol.* **1926**, *34*, 577–590. [[CrossRef](#)]
19. Poland, J.F.; Davis, G.H. Land subsidence due to withdrawal of fluids. *Rev. Eng. Geol.* **1969**, *2*, 187–270.
20. Bell, F.G.; Cripps, J.C.; Culshaw, M.G. A review of the engineering behavior of soils and rocks with respect to groundwater. *Geol. Soc. Eng. Geol. Spec.* **1986**, *3*, 1–23.
21. Shi, X.Q.; Xue, Y.Q.; Ye, S.J.; Wu, J.C.; Zhang, Y.; Yu, J. Characterization of land subsidence induced by groundwater withdrawals in Su-Xi-Chang area, China. *Environ. Geol.* **2007**, *52*, 27–40. [[CrossRef](#)]
22. Inaba, Y.; Abe, I.; Iwasaki, S.; Aoki, S.; Endo, T.; Kaido, R. Review of land subsidence researches in Tokyo. In Proceedings of the Tokyo Symposium in Land Subsidence, Tokyo, Japan, 1 September 1969; pp. 87–98.
23. Perlman, H. United States Geological Survey. Land Subsidence. Available online: <http://water.usgs.gov/edu/earthgwlandsubside.html> (accessed on 24 February 2017).
24. Pandey, V.P.; Shrestha, S.; Kazama, F. Groundwater in the Kathmandu Valley: Development dynamics, consequences and prospects for sustainable management. *Eur. Water* **2012**, *37*, 3–14.
25. 2998-NEP: *Urban Water Supply Reforms in the Kathmandu Valley*; Inc. Metcalf & Eddy: Houston, TX, USA; CEMAT Consultants Ltd.: Kathmandu, Nepal, 2000; Volume I–II.
26. Shrestha, S.; Semkuyu, D.J.; Pandey, V.P. Assessment of groundwater vulnerability and risk to pollution in Kathmandu Valley. *Nepal. Sci. Total Environ.* **2016**, *556*, 23–35. [[CrossRef](#)] [[PubMed](#)]
27. Rana, G.; Murray, A.B.; Maharjan, D.R.; Thaku, A.K. *Kathmandu Valley Environmental Outlook*; International Centre for Integrated Mountain Development (ICIMOD): Kathmandu, Nepal, 2007.
28. Pradhanang, S.M.; Shrestha, S.D.; Steenhuis, T.S. Comprehensive review of groundwater research in the Kathmandu Valley, Nepal. In *Kathmandu Valley Groundwater Outlook*; Shrestha, S., Pradhananga, D., Pandey, V.P., Eds.; Asian Institute of Technology (AIT): Klong Luang, Thailand; Small Earth Nepal (SEN): Kathmandu, Nepal; Center of Research for Environment Energy and Water (CREEW): Kathmandu, Nepal; International Research Center for River Basin Environment-University of Yamanashi: Kofu, Japan, 2012; pp. 6–18.
29. Kobayashi, T.; Morishita, Y.; Yurai, H. Detailed crustal deformation and fault rupture of 2015 Gorkha earthquake, Nepal, revealed from ScanSAR-based interferograms of ALOS-2. *Earth Planets Sp.* **2015**, *67*. [[CrossRef](#)]
30. Elliot, J.R.; Jolivet, R.; Gonzalez, P.J.; Avouc, J.P.; Hollingsworth, J.; Searle, M.P.; Stevens, V.L. Himalayan megathrust geometry and relation to topography revealed by the Gorkha earthquake. *Nat. Geosci.* **2016**, *9*, 174–180. [[CrossRef](#)]
31. Diao, F.; Walter, T.R.; Motagh, M.; Prats-Iraola, P.; Wang, R.; Samsonov, S.V. The 2015 Gorkha earthquake investigated from radar satellites: Slip and stress modeling along the MHT. *Front. Earth Sci.* **2015**, *3*, 65. [[CrossRef](#)]
32. Lavé, J.; Yule, D.; Sapkota, S.; Basant, K.; Madden, C.; Attal, M.; Pandey, R. Evidence for a great medieval earthquake (approximate to 1100 AD) in the Central Himalayas. *Nepal. Sci.* **2005**, *307*, 1302–1305.
33. Sapkota, S.N.; Bollinger, L.; Klinger, Y.; Tapponnier, P.; Gaudemer, Y.; Tiwari, D. Primary surface ruptures of the great Himalayan earthquakes in 1934 and 1255. *Nat. Geosci.* **2013**, *6*, 71–76. [[CrossRef](#)]
34. Avouac, J.P.; Bollinger, L.; Lave, J.; Cattin, R.; Flouzat, M. Seismic cycle in the Himalayas. *C. R. Acad. Sci. II A.* **2001**, *333*, 513–529.
35. Mugnier, J.L.; Gajurel, A.; Huyghe, P.; Jayangondaperumal, R.; Jouanne, F.; Upreti, B. Structural interpretation of the great earthquakes of the last millennium in the central Himalaya. *Earth-Sci. Rev.* **2013**, *127*, 30–47. [[CrossRef](#)]

36. Luo, H.; Chen, T. Three Dimensional Surface Displacement Field Associated with the 25 April 2015 Gorkha, Nepal Earthquake: Solution from Integrated InSAR and GPS Measurements with an Extended SISTEM Approach. *Remote Sens.* **2016**, *8*, 599. [[CrossRef](#)]
37. Tomás, R.; Romero, R.; Mulas, J.; Marturia, J.J.; Mallorqui, J.J.; Lopez-Sanchez, J.M.; Herrera, G.; Gutierrez, F.; Gonzalez, P. J.; Fernandez, J.; et al. Radar interferometry techniques for the study of ground subsidence phenomena: A review of practical issues through cases in Spain. *Environ. Earth Sci.* **2014**, *71*, 163–181. [[CrossRef](#)]
38. Galloway, D.L.; Hudnut, K.W.; Ingebritsen, S.E.; Phillips, S.P.; Peltzer, G.; Rogez, F.; Rosen, P.A. Detection of aquifer system compaction and land subsidence using interferometric synthetic aperture radar, Antelope Valley, Mojave Desert, California. *Water Resour. Res.* **1998**, *34*, 2573–2585. [[CrossRef](#)]
39. Sneed, M.; Ikeheara, M.E.; Galloway, D.L.; Amelung, F. *Detection and Measurement of Land Subsidence Using Global Positioning System and Interferometric Synthetic Aperture Radar, Coachella Valley, California, 1996–98*; Water Resources Investigation Report 01-4193; U.S. GEOLOGICAL SURVEY: Sacramento, CA, USA.
40. Chatterjee, R.S.; Fruneau, B.; Rudant, J.P.; Roy, P.S.; Frison, P.; Lakhera, R.C.; Dadhwal, V.K.; Saha, R. Subsidence of Kolkata (Calcutta) City, India during the 1990s as observed from space by Differential Synthetic Aperture Radar Interferometry (D-InSAR) technique. *Remote Sens. Environ.* **2006**, *102*, 176–185. [[CrossRef](#)]
41. Motagh, M.; Walter, T.R.; Sharifi, M.A.; Fielding, E.; Schenk, A.; Anderssohn, J.; Zschau, J. Land subsidence in Iran caused by widespread water reservoir overexploitation. *Geophys. Res. Lett.* **2008**, *35*, L16403. [[CrossRef](#)]
42. Bayuaji, L.; Josaphat, T.S.S.; Kuze, H. ALOS PALSAR D-InSAR for land subsidence mapping in Jakarta, Indonesia. *Can. J. Remote Sens.* **2010**, *36*, 1–8. [[CrossRef](#)]
43. Boni, R.; Herrera, G.; Meisina, C.; Notti, D.; Béjar-Pizarro, M.; Zucca, F.; González, P.J.; Palano, M.; Tomás, R.; Fernández, J.; Fernández-Merodo, J.A.; et al. Twenty-year advanced DInSAR analysis of severe land subsidence: The Alto Guadalentín Basin (Spain) case study. *Eng. Geol.* **2015**, *198*, 40–52. [[CrossRef](#)]
44. Abidin, H.Z.; Andreas, H.; Gamal, M.; Djaja, R.; Subarya, C.; Hirose, K.; Maruyama, Y.; Murdohardono, D.; Rajiyowiryono, H. Monitoring land subsidence of Jakarta (Indonesia) using levelling, GPS survey and InSAR techniques. *Int. Assoc. Geod. Symp.* **2005**, *128*, 561–566.
45. Cascini, L.; Ferlisi, S.; Fornaro, G.; Lanari, R.; Peduto, D.; Zeni, G. Subsidence monitoring in Sarno urban area via multi-temporal DInSAR technique. *Int. J. Remote Sens.* **2006**, *27*, 1709–1716. [[CrossRef](#)]
46. Chini, M.; Bignami, C.; Stramondo, S.; Pierdicca, N. Uplift and subsidence due to the 26 December 2004 Indonesian earthquake detected by SAR data. *Int. J. Remote Sens.* **2008**, *29*, 3891–3910. [[CrossRef](#)]
47. Guoqing, Y.; Jingquin, M. DInSAR technique for land subsidence monitoring. *Earth Sci. Front.* **2008**, *15*, 239–243. [[CrossRef](#)]
48. Yan, Y.; Doin, M.P.; Lopez-Quiroz, P.; Tupin, F. Mexico City subsidence measured by InSAR time series: Joint analysis using PS and SBAS approaches. *IEEE J. Sel. Top. App. Earth Obs. Remote Sens.* **2012**, *5*, 1312–1326. [[CrossRef](#)]
49. Amelung, F.; Galloway, D.L.; Bell, J.W.; Zebker, H.A.; Lacznia, R.J. Sensing the ups and downs of Las Vegas: InSAR reveals structural control of land subsidence and aquifer-system deformation. *Geology* **1999**, *27*, 483–486. [[CrossRef](#)]
50. Calo, F.; Abdikan, S.; Gorum, T.; Pepe, A.; Kilic, H.; Sanli, F.B. The space-borne SBAS-DInSAR technique as a supporting tool for sustainable urban policies: The case of Istanbul Megacity, Turkey. *Remote Sens.* **2015**, *7*, 16519–16536. [[CrossRef](#)]
51. Pandey, M.R. Ground response of Kathmandu valley on the basis of microtremors. In Proceedings of the World Conference on Earthquake Engineering, Auckland, New Zealand, 30 January–4 February 2000.
52. Piya, B.K. Generation of a Geological Database for the Liquefaction Hazard Assessment in Kathmandu Valley. Master's Thesis, International Institute for Geo-Information Science and Earth Observation, Enschede, The Netherlands, 2004.
53. Nautiyal, S.P.; Sharma, P.N. A Geological Report on the Groundwater Investigation of Kathmandu Valley. Unpublished work. 1961.
54. Moribayashi, S.; Maruo, Y. Basement topography of Kathmandu Valley, Nepal: An application of gravitational method to the survey of a tectonic basin in the Himalayas. *J. Japan Soci. Eng. Geol.* **1980**, *21*, 30–37. [[CrossRef](#)]

55. Stocklin, J.; Bhattarai, K.D. Geology of Kathmandu Area and central Mahabharat Range, Nepal Himalaya. HMG/UNDP Mineral Exploration Project, Kathmandu. Unpublished work. 1977.
56. Kuwahara, Y.; Masudome, Y.; Paudel, M.R.; Fuji, R.; Hayashi, T.; Mampuku, M.; Sakai, H. Controlling weathering and erosion intensity on the southern slope of the central Himalaya by the Indian summer monsoon during the last glacial. *Glob. Planet. Chang.* **2010**, *71*, 73–84. [[CrossRef](#)]
57. Ardiansyah. *Tutorial InSAR Menggunakan Sarscape*; Department of Geography, University of Indonesia: Depok, Indonesian, Unpublished work; 2013; p. 8.
58. Yerro, A.; Corominas, J.; Monells, D.; Mallorqui, J.J. Analysis of the evolution of ground movements in a low densely urban area by means of DInSAR technique. *Eng. Geol.* **2014**, *170*, 52–56. [[CrossRef](#)]
59. Curlander, J.C.; McDonough, R.N. *Synthetic Aperture Radar: Systems and Signal Processing*; Wiley-Interscience: Toronto, ON, Canada, 1991.
60. Exelis Help Article: Estimating the Appropriate Number of Looks When Multilooking Images in SARscape. Available online: <http://www.harrisgeospatial.com/Support/HelpArticles/TabId/185/ArtMID/800/ArticleID/4265/4265.aspx> (accessed on 15 September 2014).
61. SAR Guidebook. Available online: [www.sarmap.ch/pdf/SAR-Guidebook.pdf](http://www.sarmap.ch/pdf/SAR-Guidebook.pdf) (accessed on 16 August 2010).
62. Goldstein, R.M.; Werner, C.L. Radar interferogram filtering for geophysical applications. *Geophys. Res. Lett.* **1998**, *25*, 4035–4038. [[CrossRef](#)]
63. Anderssohn, J.; Wetzell, H.U.; Walter, T.R.; Motagh, M.; Djamour, Y.; Kaufmann, H. Land subsidence pattern controlled by old alpine basement faults in the Kashmar Valley, Northeast Iran: Results from InSAR and levelling. *Geophys. J. Int.* **2008**, *174*, 287–294. [[CrossRef](#)]
64. Thrall, G.I. *Business Geography and New Real Estate Market Analysis*; Oxford University Press: Oxford, UK, 2000; p. 216.
65. Sato, H.P.; Abe, K.; Ootaki, O. GPS-measured land subsidence in Ojiya City, Niigata Prefecture, Japan. *Eng. Geol.* **2003**, *67*, 379–390. [[CrossRef](#)]
66. Sakai, H. Stratigraphic division and sedimentary facies of the Kathmandu Basin group, Central Nepal. *J. Nepal Geol. Soc.* **2001**, *25*, 19–32.
67. Shrestha, S.R.; Shah, S. Shallow Aquifer Mapping of Kathmandu Valley. Groundwater Resources Development Board, Babarmahal, Kathmandu. Available online: [http://www.academia.edu/27155659/Shallow\\_Aquifer\\_Mapping\\_of\\_Kathmandu\\_Valley](http://www.academia.edu/27155659/Shallow_Aquifer_Mapping_of_Kathmandu_Valley) (accessed on 23 February 2017).
68. Pathak, D.R.; Hiratsuka, A. An investigation of nitrate and iron concentrations and their relationship in shallow groundwater systems of Kathmandu. *Desalination Water Treat.* **2010**, *19*, 191–197. [[CrossRef](#)]



© 2017 by the authors. Licensee MDPI, Basel, Switzerland. This article is an open access article distributed under the terms and conditions of the Creative Commons Attribution (CC BY) license (<http://creativecommons.org/licenses/by/4.0/>).